DOI: 10.1002/ejic.200600946

Factors Affecting the Interlayer Arrangement of Transition Metal–Ethylenediaminetetraacetate Complexes Intercalated in Mg/Al Layered Double Hydroxides

Guoqing Wu,[a] Lianying Wang,*[a] Lan Yang,[a] and Junjiao Yang[a]

Keywords: Layered compounds / Intercalation / Metal–edta complexes / Reorientation / Organic–inorganic hybrid composites

Transition metal (M)–ethylenediaminetetraacetate (edta) complexes {$[M(edta)]^{2-}$} have been intercalated in layered double hydroxides (LDHs) by a hydrothermal method using $MgAl–NO_3$ LDH as the precursor. The factors affecting the orientation of the incorporated $[M(edta)]^{2-}$ in the resulting well-ordered materials were investigated. Whilst varying the metal cation in the intercalated complex has no major influence on the orientation of the $[M(edta)]^{2-}$ (M = Co, Ni, Cu, Zn) anion in the interlayer galleries, there is a marked dependence on layer charge density. The observed basal spacings of 1.402–1.461 nm for Mg_2Al–M(edta) LDH and 1.254 nm for Mg_3Al–Zn(edta) LDH can be ascribed to bilayer and monolayer arrangements, respectively, of the $[M(edta)]^{2-}$ anion. When the Mg/Al ratio is varied in the range 2.2–2.7 the two guest arrangements coexist. The evolution of the interlayer arrangement of $[M(edta)]^{2-}$ in LDHs with increasing temperature was studied by variable-temperature in-situ XRD measurements, variable-temperature in-situ FT-IR, and combined thermogravimetric analysis and mass spectrometry (TGA-MS). In the case of Mg_2Al–M(edta) LDH, a metastable phase with a similar monolayer structure to that found in Mg_3Al–M(edta) LDH was detected by XRD in the range 140–300 °C. Cooling of the calcined solid to room temperature in air leads to the recovery of the original bilayer structure. The reversible nature of the structural transformation indicates that a reorientation of the guest $[M(edta)]^{2-}$ complex in the interlayer galleries occurs on heating, rather than a grafting process. Heat treatment of Mg_3Al–M(edta) LDH results only in a gradual contraction of the basal spacing associated with the loss of interlayer water without any reorientation of the guest $[M(edta)]^{2-}$ complex.

Introduction

By virtue of their anion-exchange properties, layered double hydroxides (LDHs) have potential applications as catalysts or precursors to new catalytic materials, such as ion exchangers, adsorbents, or hosts for nanoscale reactions as well as in medicine.[1] LDHs can be represented by the general formula $[M^{II}_{1-x}M^{III}_{x}(OH)_2]^{x+}(A^{n-})_{x/n}\cdot yH_2O$. Their structure is based on the stacking of positively charged layers arising from the substitution of trivalent cations for part of the divalent cations in brucite-like layers, and exchangeable anions (A^{n-}) in hydrated interlayer galleries.

In recent years, great attention has been paid to the intercalation of metal complex anions in LDHs in an effort to develop new functional materials such as heterogeneous catalysts, photocatalytic materials, magnetic nanocomposites, and luminescent materials.[2–5] In particular, intercalation of metal–edta complexes into LDHs has been extensively studied due to the strong chelating ability of the edta ligand with almost any metal cation.[6–14] O'Hare et al.[6] have recently prepared LDHs containing such complexes, either directly by intercalation of the transition metal–edta complex or indirectly by forming the metal complex in situ in the interlayer galleries of Li–Al LDH pre-intercalated with edta. Tsyganok et al.[7] have studied the catalytic activity in dry reforming of methane of a material derived from LDH-intercalated $[Ni(edta)]^{2-}$ complexes. Lukashin et al.[3] have reported the magnetic properties of anisotropic metal nanoparticles prepared from an LDH containing an edta complex of Fe^{III} or Ni^{II}. The synthesis and characterization of an Mg_2Al LDH intercalated by luminescent $[Eu(edta)]^-$ complexes was recently reported.[8]

In general, the arrangement of interlayer guest anions can dramatically influence the physicochemical properties of LDH materials.[15–18] For example, in the case of poly(diacetylenecarboxylates) incorporated in LDHs, the possibility of having different arrangements of interlayer guests is responsible for the observed reversible thermal color changes.[18] In developing such functional materials it is important to be able to control the orientation of functional guest anions in the interlayer galleries in order to fully uti-

[a] State Key Laboratory of Chemical Resource Engineering, Beijing University of Chemical Technology,
Box 98, 15 Beisanhuan Dong Lu, Beijing 100029, China
Fax: +86-1064425385
E-mail: wangliany@mail.buct.edu.cn

lize their anisotropic properties. An understanding of the factors controlling the interlayer arrangement is important if tailored applications in areas such as those mentioned above are to be found for LDHs containing $[M(edta)]^{2-}$ complexes, but no such study has been reported to date.

In addition, thermal treatment is a key step in the synthesis of LDH-derived catalysts. Despite numerous investigations of the structural evolution of LDHs with temperature the process of thermal decomposition of LDHs, in particular the origin of thermally metastable intermediate phases, is still a matter of debate. The possible role of grafting simple or complex anions to the slabs in the formation of the thermally metastable phase has been extensively discussed. Whilst a grafting phenomenon at low temperature has been reported for LDHs with both oxygen-containing and non-oxygen-containing anions,[19–24] other authors have suggested that the thermally metastable phase originates from a reorientation of the anions in the interlayer domains rather than from such a grafting process.[25–30]

In this work, we report the intercalation of transition metal complexes $[ZnY]^{2-}$, $[NiY]^{2-}$, $[CoY]^{2-}$, and $[CuY]^{2-}$ (where Y denotes $edta^{4-}$) into MgAl LDHs with different Mg/Al ratios, by a hydrothermal synthesis method. Our aim is to clarify the factors affecting the orientation of the complexes, particularly in the temperature interval 30–400 °C, in order to understand the evolution of the interlayer phase with temperature. Structural changes arising from thermal treatment are monitored by variable-temperature in-situ XRD, variable-temperature in-situ FT-IR, and combined thermogravimetric analysis and mass spectrometry (TGA-MS). Such information should enable a better understanding of the LDH–M(edta) structure and provide a framework for the synthesis of new functional materials.

Results and Discussion

Three methods for the intercalation of the $[MY]^{2-}$ complex in LDH materials, namely ion exchange, coprecipitation, and reconstruction, have been described in the literature. In order to obtain a pure LDH phase containing the $[MY]^{2-}$ complex, a large (tenfold) excess of the $[MY]^{2-}$ complex has typically been employed.[3,7] If the amount of $[MY]^{2-}$ complex is low it has been reported that the materials suffer from poor crystallinity and the coexistence of more than one phase, which makes it impossible to study their structures in detail.[8,31] In an attempt to overcome this problem we chose to employ a hydrothermal synthesis using only a twofold excess of the $[MY]^{2-}$ complex.

Effect of Varying the Metal Cation in the Complex Anion on Interlayer Orientation

Chemical analysis (see Table 1) confirms both that the nitrate anions in the LDH-2.0-NO_3 precursor have been completely exchanged by anionic edta complexes and that there is no contamination by co-intercalated carbonate ions. The composition of the LDH-2.0-NO_3 precursor (where 2.0 refers to the Mg^{2+}/Al^{3+} molar ratio in the synthesis mixture) and intercalated materials are given in Table 1. The Mg/Al molar ratio in LDH-2.0-[MY] (M = Zn, Ni, Co, Cu) is essentially the same as that in the LDH-2.0-NO_3 precursor (2.04), which excludes the possibility of partial dissolution of the magnesium in the layers during the hydrothermal synthesis.

The XRD patterns of the LDH-2.0-NO_3 precursor and its exchanged products (LDH-2.0-[MY]) are shown in Figure 1. The patterns are typical of lamellar materials, with a basal reflection and associated harmonics at low angles 2θ and weaker nonbasal reflections at higher angles. Intercalation of $[MY]^{2-}$ leads to an increase in basal spacing for all the exchanged LDHs and the values of the basal spacing in LDH-2.0-[MY] (M = Zn, Cu, Co) are rather similar, whilst that for LDH-2.0-[NiY] is slightly lower (see Table 1). This is indicative of a similar orientation of the $[MY]^{2-}$ anions within the interlayer galleries. No change is observed in the value of the unit cell parameter *a*, calculated from the posi-

Table 1. Chemical composition, cell parameter *a*, and basal spacing *d*(003) for the LDH materials.

Sample	Mg/Al	Chemical composition (found/calcd.) [wt-%] and proposed formula	*a* [nm]	*d*(003) [nm]
LDH-2.0-[NO_3]	2.04	Mg 18.58/18.51, Al 10.27/10.11, N 5.14/5.24, H 3.25/3.34 $[Mg_{0.68}Al_{0.33}(OH)_2](NO_3)_{0.33}\cdot 0.47H_2O$	0.303(0)	0.867
LDH-2.0-[ZnY]	2.03	Mg 12.45/12.50, Al 6.89/6.84, Zn 8.27/8.38, C 15.21/15.38, N 3.61/3.70, H 4.23/4.15 $[Mg_{0.67}Al_{0.33}(OH)_2][Zn(C_{10}H_{12}N_2O_8)]_{0.16}\cdot 0.71H_2O$	0.302(8)	1.445
LDH-2.0-[NiY]	2.00	Mg 12.52/12.57, Al 7.03/6.97, Ni 7.63/7.57, C 15.39/15.48, N 3.68/3.61, H 4.15/4.13 $[Mg_{0.67}Al_{0.33}(OH)_2][Ni(C_{10}H_{12}N_2O_8)]_{0.16}\cdot 0.65H_2O$	0.302(7)	1.402
LDH-2.0-[CuY]	2.01	Mg 12.38/12.25, Al 6.94/6.89, Cu 8.05/8.10, C 15.23/15.30, N 3.64/3.57, H 4.25/4.16 $[Mg_{0.66}Al_{0.33}(OH)_2][Cu(C_{10}H_{12}N_2O_8)]_{0.16}\cdot 0.70H_2O$	0.302(8)	1.461
LDH-2.0-[CoY]	1.99	Mg 12.41/12.29, Al 6.97/6.90, Co 7.50/7.53, C 15.18/15.30, N 3.67/3.58, H 4.31/4.21 $[Mg_{0.66}Al_{0.33}\ (OH)_2][Co(C_{10}H_{12}N_2O_8)]_{0.16}\cdot 0.73H_2O$	0.303(1)	1.440
LDH-2.2-[ZnY]	2.19	Mg 13.60/13.65, Al 6.96/6.90, Zn 8.02/8.09, C 14.91/14.84, N 3.52/3.46, H 4.05/3.99 $[Mg_{0.69}Al_{0.31}(OH)_2][Zn(C_{10}H_{12}N_2O_8)]_{0.15}\cdot 0.52H_2O$	0.303(2)	1.401
LDH-2.5-[ZnY]	2.46	Mg 14.70/14.66, Al 6.72/6.64, Zn 7.69/7.77, C 14.34/14.26, N 3.55/3.45, H 4.10/3.94 $[Mg_{0.72}Al_{0.29}(OH)_2][Zn(C_{10}H_{12}N_2O_8)]_{0.14}(NO_3)_{0.02}\cdot 0.48H_2O$	0.303(3)	1.350
LDH-2.7-[ZnY]	2.72	Mg 15.51/15.41, Al 6.43/6.41, Zn 6.94/6.90, C 12.58/12.66, N 3.40/3.32, H 4.01/4.06 $[Mg_{0.73}Al_{0.27}\ (OH)_2][Zn(C_{10}H_{12}N_2O_8)]_{0.12}(NO_3)_{0.03}\cdot 0.59H_2O$	0.303(5)	1.299
LDH-3.0-[ZnY]	2.97	Mg 16.50/16.48, Al 6.26/6.18, Zn 5.91/5.82, C 11.09/10.98, N 3.28/3.20, H 4.25/4.16 $[Mg_{0.75}Al_{0.25}(OH)_2][Zn(C_{10}H_{12}N_2O_8)]_{0.10}(NO_3)_{0.05}\cdot 0.67H_2O$	0.304(2)	1.254

tion of the $d(110)$ reflection near $2\theta = 60°$, suggesting that the average cation–cation distance in the layers of LDH-2.0-[MY] remains unaffected (Table 1). This is consistent with the result from chemical analysis. An inversion of the relative intensities between the (006) and (009) reflections in the XRD pattern of LDH-2.0-[MY] is observed relative to those in the LDH-2.0-NO_3 precursor. This phenomenon has been ascribed to the presence of atoms with large scattering power in the interlayer region.[2,25] This will be discussed in detail below. The observation that the Mg/Al ratio in the layers is not affected by the incorporation of the edta complexes and that the orientation of the anions within the interlayer galleries is essentially independent of the identity of the metal M may be attributed to the similar coordination mode and high stability constants of the metal–edta complexes.[32,33]

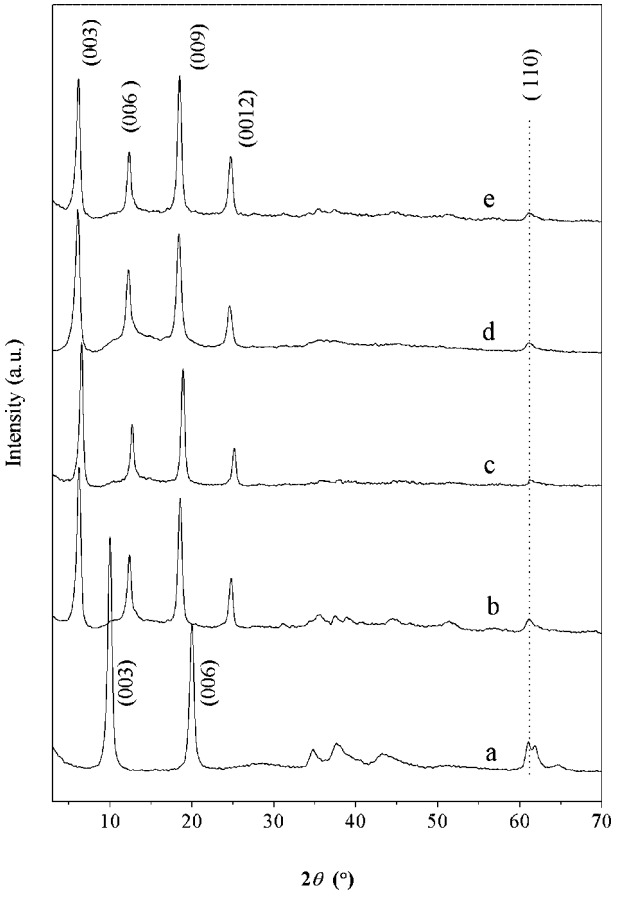

Figure 1. Powder XRD patterns of (a) LDH-2.0-NO_3, (b) LDH-2.0-[ZnY], (c) LDH-2.0-[NiY], (d) LDH-2.0-[CuY], and (e) LDH-2.0-[CoY].

The LDH materials were also characterized by FT-IR and selected spectra are shown in Figure 2. For the LDH nitrate precursor (Figure 2a), the intense and broad absorption band centered at 3445 cm^{-1} corresponds to the stretching vibrations of the hydroxyl groups of both the layer hydroxide moieties and interlayer water molecules. The broadening of this band is due to hydrogen-bond formation.[34] The band close to 1640 cm^{-1} corresponds to the deformation mode (δH_2O) of water molecules. The absorption peaks at 1384 and 839 cm^{-1} are usually assigned to the ν_3 and ν_2 vibration modes, respectively, of NO_3^- with D_{3h} symmetry,[35] whilst bands around 447 and 675 cm^{-1} are from Al–O and Mg–O lattice vibrations, respectively.[36]

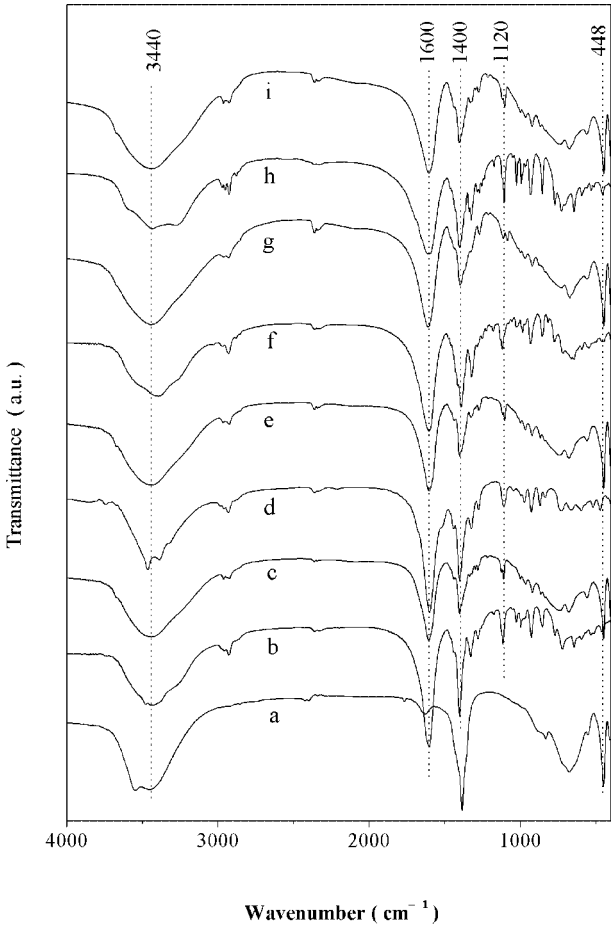

Figure 2. FT-IR spectra of (a) LDH–NO_3-2.0, (b) Na_2[ZnY], (c) LDH-2.0-[ZnY], (d) Na_2[NiY] (e) LDH-2.0-[NiY], (f) Na_2[CuY], (g) LDH-2.0-[CuY], (h) Na_2[CoY], and (i) LDH-2.0-[CoY].

After exchange of Mg_2Al–NO_3 LDH with Na_2[MY]·$3H_2O$ the ν_3 vibration of NO_3^- disappears, and the asymmetric ν_{as}(COO) and symmetric ν_s(COO) stretching modes of the carboxylate groups, at 1600 and 1400 cm^{-1}, respectively, appear (Figure 2c). The wavenumber difference $\Delta\nu = \nu_{as} - \nu_s$ gives information about the coordination environment of the carboxylate group.[37,38] The value of $\Delta\nu$ in both Na_2[MY]·$3H_2O$ and LDH-2.0-[MY] is greater than 200 cm^{-1}, indicating the presence of deprotonated carboxylate groups coordinated to the metal ion in a monodentate fashion.[37,38] Furthermore, the similar values of $\Delta\nu$ for LDH-2.0-[MY] and Na_2[MY]·$3H_2O$ suggest that the coordination mode of the carboxylate groups is unchanged after intercalation. The slight difference in the value of $\Delta\nu$ may be a reflection of the different intermolecular hydrogen-bonding environments experienced by the anion in the sodium salt and in the interlayer galleries of the LDH.[38–40] This result clearly confirms the presence of $[MY]^{2-}$ anions between the layers.

Effect of Varying the Layer Charge Density on the Orientation of the Guest Anions

The layer charge density is often an important factor in determining the orientation of the guest anions in the interlayer galleries.[16,41] For further insight into the structure of the LDH-intercalated $[MY]^{2-}$ complexes samples of LDH-*X*-[ZnY] (with Mg/Al ratio in the synthesis mixture $X = 2.0$, 2.2, 2.5, 2.7, 3.0) were chosen. Elemental compositions of the resulting LDH-*X*-[ZnY] materials are given in Table 1. The Mg/Al molar ratios in LDH-*X*-[ZnY] are essentially the same as those in the corresponding LDH-*X*-NO_3 precursors (not shown in Table 1) which excludes the possibility of partial dissolution of the magnesium in the layers during the hydrothermal synthesis. Elemental analysis confirms that small amounts of NO_3^- anion are co-intercalated with $[ZnY]^{2-}$ at high Mg/Al molar ratios, suggesting that intercalation of the bulky $[ZnY]^{2-}$ anion becomes less favorable as the layer-charge density decreases.[41,42]

The XRD results of LDH-*X*-[ZnY] (see Figure 3) show that there is not only a progressive decrease in the basal spacing for samples from 1.445 nm in LDH-2.0-[ZnY] (Figure 3a) to 1.254 nm in LDH-3.0-[ZnY] (Figure 3e) but also a significant variation in the relative intensities of the (00*l*) (l = 3, 6, 9, 12) reflections with the Mg/Al mol ratio, suggesting different orientations of $[MY]^{2-}$ within the interlayer galleries. In general, when atoms with large scattering power are located at different positions along the *c* axis, the usual pattern of decreasing intensities of successive (00*l*) reflections with increasing *l* is not observed because of the fluctuations in the one-dimensional electron-density distribution along the *c* axis.[2,4,25,43–45] When the intensity of the (006) reflection is greater than that of (003), as is the case for LDH-3.0-[ZnY], it has been proposed that the heavy metal atom is located at the midpoint of the interlayer galleries.[2,4,25,44] In LDH-2.0-[ZnY], the intensity of the (009) reflection is greater than that of (006), suggesting that the alternate heavy metal centers are located above and below the midpoint of the interlayer galleries.[4,43,45]

When the Mg/Al molar ratio is increased to 2.2 no significant changes are observed (Figure 3b), suggesting there is only a single phase corresponding to a basal spacing of 1.445 nm. However, on further increasing the Mg/Al molar ratio, LDH-2.5-[ZnY] shows a complicated pattern of broad XRD reflections suggesting that two or more phases (Figure 3c), with different basal spacings, are present; the intensity of the third harmonic reflection (009) also decreases much more than that of the other (00*l*) reflections. These results indicate that some variation in the arrangement of the guest anions is associated with the decrease in layer-charge density. In the case of LDH-2.7-[ZnY] (see Figure 3d), the asymmetric (00*l*) reflections and the splitting of the (006) reflection are also consistent with the presence of at least two LDH phases. When the Mg/Al molar ratio is increased to 3.0, with the exception of a weak shoulder on the (006) reflection peak centered at $2\theta \approx 12°$, the reflections are characteristic of a single phase with a basal spacing of 1.254 nm. The elemental analysis results also

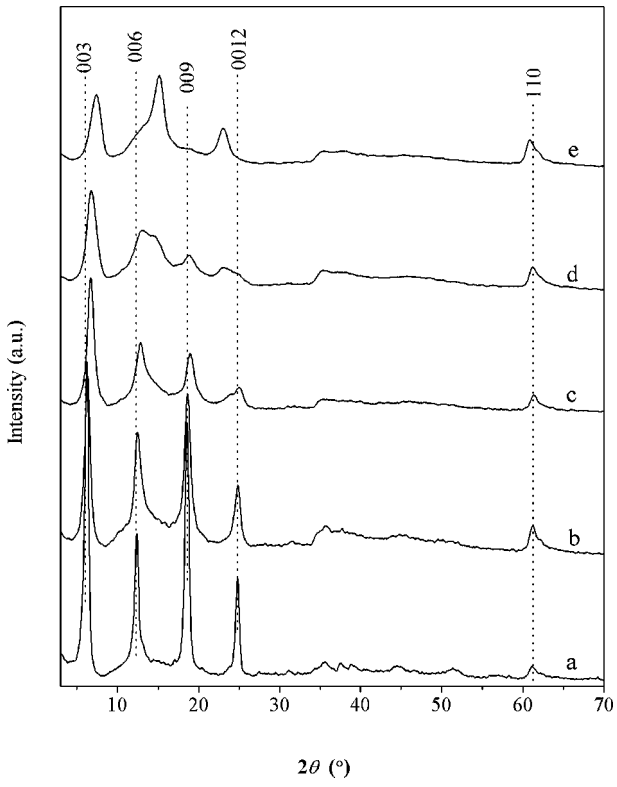

Figure 3. Powder XRD patterns of (a) LDH-2.0-[ZnY], (b) LDH-2.2-[ZnY], (c) LDH-2.5-[ZnY], (d) LDH-2.7-[ZnY], and (e) LDH-3.0-[ZnY].

show that LDH-3.0-[ZnY] in contrast to LDH-2.0-[ZnY] contains a significant amount of NO_3^-. This can perhaps also contribute to the asymmetric shape of the peaks in the XRD pattern of the former sample. The XRD data suggest that the phase LDH-2.0-[ZnY] involves the heavy metal centers located alternately above and below the midpoint of the interlayer galleries and the phase LDH-3.0-[ZnY] has the heavy metal centers located at the midpoint of the interlayer galleries. For intermediate Mg/Al molar ratios (2.2–2.7) the two LDH phases are both present; there is no evidence for a new phase with a third guest arrangement in LDH–[ZnY].

Structural Model for LDH–MY

The observed basal spacings are 1.445 nm in LDH-2.0-[ZnY] and 1.254 nm in LDH-3.0-[ZnY], respectively. If the thickness of the LDH layer is taken as 0.48 nm,[46] the gallery heights are 0.97 nm and 0.77 nm, respectively. A gallery height of 0.97 nm is in close agreement with the maximal dimensions (0.90–1.00 nm) of the complex anion in salts such as $K_2[CuY]\cdot 3H_2O$, $Ca[NiY]\cdot 4H_2O$, and $Ca[Co(H_2O)Y]\cdot 4H_2O$ as determined by single-crystal XRD.[32,23] On this basis O'Hare et al.[6] proposed that the interlayer of $LiAl_2$–[MY] LDH consists of a monolayer of metal–edta complexes with the maximal dimension of each anion perpendicular to the hydroxide layers. This model, with the heavy

metal atom located at the midpoint of the interlayer galleries, is not consistent with the observed inversion of the relative intensities between the (006) and (009) reflections in the LDH-2.0-[MY]. However, this indicates that the heavy metal atom is located at sites alternately above and below the midpoint of the interlayer galleries in LDH-2.0-[MY], as discussed above.

A gallery height of 0.97 nm in LDH-2.0-[ZnY] is, however, almost twice as long as the minimal dimensions (0.5 nm) of the complex anion in the above salts.[32,33] Therefore it is reasonable to assume that the interlayer galleries consist of a condensed bilayer of guest species with the minimal dimension of each anion perpendicular to the brucite-like layers in the LDH-2.0-[ZnY], as shown schematically in Figure 4a. In this model the four carboxylate groups of individual anions all interact with the same hydroxide layer, maximizing the interaction with the layers through both electrostatic attractions with the positive charge and hydrogen bonding with the layer hydroxyl groups. The inversion of the relative intensities between the (006) and (009) reflections in the XRD pattern of LDH-2.0-[ZnY] is consistent with this model of a bilayer arrangement of $[ZnY]^{2-}$ guests. In the bilayer orientation, the corresponding cross-sectional area occupied by each anion in the *ab* plane is in the range 0.81–1.00 nm^2 (see Figure 4a). The area per unit charge of the host lattice with an Mg/Al ratio of 2.0, calculated from the crystallographic data, is 0.25 nm^2.[16,47] Since the guests are orientated in a bilayer (as shown in Figure 4a), the area available per two divalent anions is approximately 1.0 nm^2 (4×0.25 nm^2). It follows that in a bilayer of $[ZnY]^{2-}$ anions, the host layer charge can be balanced, although relatively close packing of guest anions in the *c* axis direction is required.

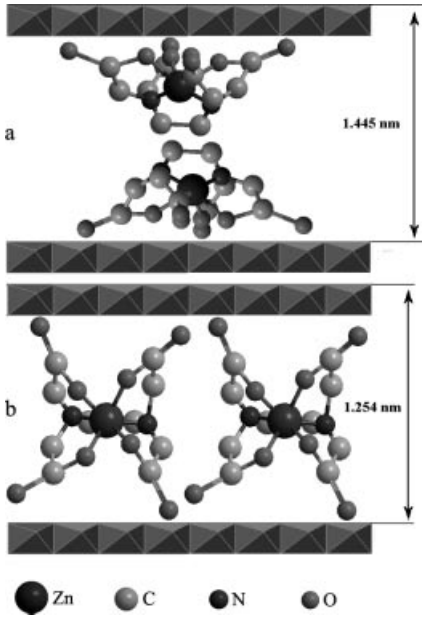

Figure 4. Schematic illustration of the structures of (a) LDH-2.0-[ZnY] and (b) LDH-3.0-[ZnY].

Taking into account the gallery height (0.77 nm) and the observed inversion of intensity between the first two (00*l*) peaks in LDH-3.0-[ZnY], we propose that in LDH-3.0-[ZnY] the metal–edta complexes form a monolayer of guest species with two carboxylate groups of individual anions attracted electrostatically to the upper hydroxide layer and the other two attracted to the lower one, as shown schematically in Figure 4b. This model also allows a favorable interaction between the four carboxylate groups of the guest and the host layers through both electrostatic attraction with the positively charged layers and hydrogen bonding with the layer hydroxyl groups. The height (0.77 nm) in LDH-3.0-[ZnY] probably arises from a monolayer assembly, with the maximal dimension of each anion tilted with respect to the hydroxide layers. Calculations show that the $[ZnY]^{2-}$ anion is capable of balancing the host layer charge of LDH-3.0-[ZnY] when arranged in a monolayer, since the cross-sectional area occupied by each anion in the *ab* plane is in the range 0.45–0.50 nm^2, whereas the area available per divalent anion is approximately 0.66 nm^2 (2×0.33 nm^2).[16,47]

The above two guest arrangements maximize the interaction between the four carboxylate groups of the guest and the host layers and this is consistent with the absence of a new phase corresponding to a third guest arrangement at intermediate Mg/Al molar ratios. Other arrangements, such as two carboxylate groups of individual anions being fixed to upper and lower hydroxide layers and the other carboxylate groups extending into the interlayer galleries without any interaction with hydroxide layers, as proposed by O& apos;Hare et al., are less likely on energetic grounds.

The monolayer and bilayer orientation observed for the guest anions in the gallery have been reported in the literature.[4,43] Benzoate anions form bilayer-like structures[41] or monofilms of interdigitated species as found for methyl orange.[17] In all cases, the preferred orientation of the guest species is such as to permit the maximum interaction of the carboxylate groups with the layers through hydrogen bonding with the layer hydroxyl groups and, at the same time, the hydrophobic aromatic groups are located at the center of the galleries as far apart as possible from the hydrophilic layer hydroxyl groups.

Reorientation of $[MY]^{2-}$ in the Interlayer Space under Thermal Treatment

The in situ variable-temperature powder X-ray diffraction patterns of LDH-2.0-[ZnY] and LDH-3.0-[ZnY] in the temperature range 30–900 °C in an ambient atmosphere are shown in Figures 5 and 6, respectively. The relationship between the *d*(003) basal spacings of LDH–[ZnY] and the temperature is shown in Figure 7. It can be observed that the basal reflections in both LDH-2.0-[ZnY] and LDH-3.0-[ZnY] move to a higher angle with increasing temperature indicating a contraction in the interlayer spacing. However, the magnitudes and evolution of the contraction observed on heating the two samples are very different (see Figure 7). A significant contraction in basal spacing (0.244 nm) is ob-

served for LDH-2.0-[ZnY] over a very small temperature range, between 110 and 140 °C, with the basal spacing remaining nearly constant before and after the transition. In contrast, LDH-3.0-[ZnY] shows only a gradual small contraction (0.082 nm) on heating from room temperature up to 150 °C, which can be associated with loss of water. TGA-MS (see below) indicates that similar amounts of water are released over the temperature range 30–150 °C for both LDH-2.0-[ZnY] and LDH-3.0-[ZnY], suggesting that the much larger contraction observed for the former cannot be ascribed to the loss of interlayer water alone. Above 140 °C the basal spacing of LDH-2.0-[ZnY] (1.201 nm) is similar to that of LDH-3.0-[ZnY] at room temperature (1.254 nm). This suggests that a reorientation of the $[MY]^{2-}$ anions in the interlayer galleries, probably induced by the loss of the interlayer water, is the real origin of the significant contraction in LDH-2.0-[ZnY].

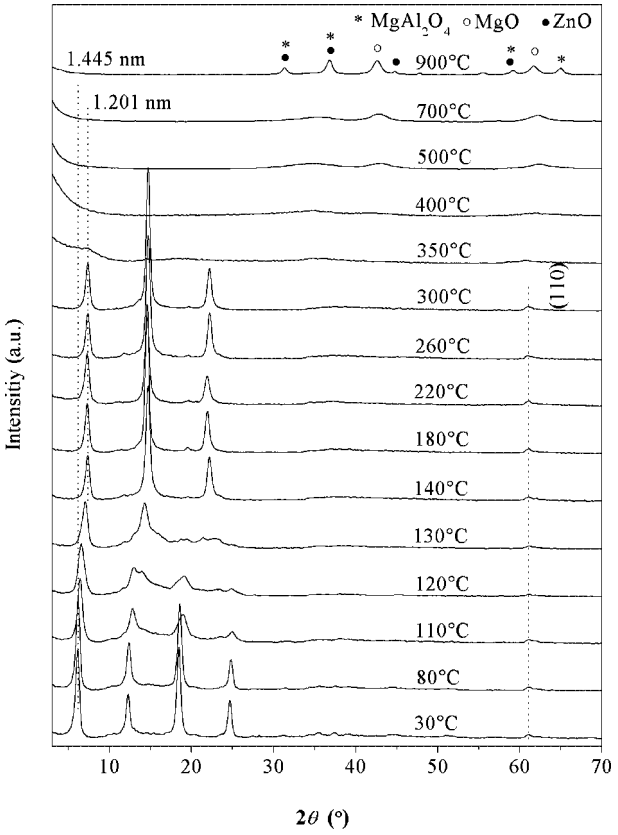

Figure 5. In-itu powder XRD patterns of LDH-2.0-[ZnY] over the temperature range 30–900 °C.

The occurrence of such a guest reorientation is confirmed by the significant variation in the relative intensities of the (00*l*) reflections in the XRD patterns of LDH-2.0-[ZnY] with increasing temperature. The inversion in intensity between the (006) peak and (009) peak in LDH-2.0-[ZnY] disappears on heating from 30 °C to 130 °C. Especially in the range 120–130 °C, the (00*l*) reflections broaden significantly and become asymmetric, which possibly corresponds to an unstable intermediate resulting from disorder in the arrangement of guests induced by loss of interlayer water from the hydrogen-bonded framework in the interlayer galleries. However, the intensity of the (006) reflections becomes significantly stronger between 140 and 300 °C and in addition a series of symmetric and strong (00*l*) reflections, with the pattern resembling that of LDH-3.0-[ZnY], emerge. Therefore it can be concluded that removal of interlayer water occurs upon heating, resulting in stronger electrostatic and hydrogen-bonding interactions between $[ZnY]^{2-}$ and LDH layer hydroxyl groups. This will

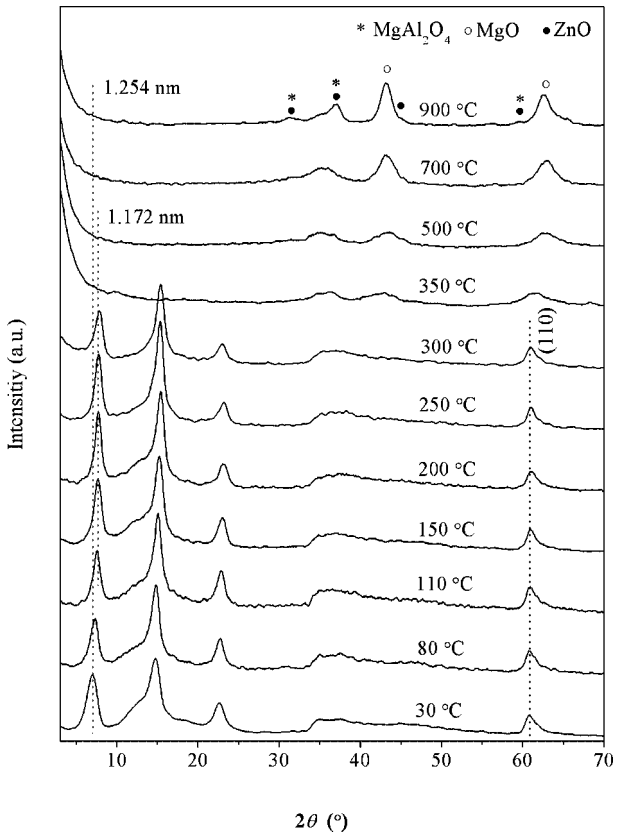

Figure 6. In-situ powder XRD patterns of LDH-3.0-[ZnY] over the temperature range 30–900 °C.

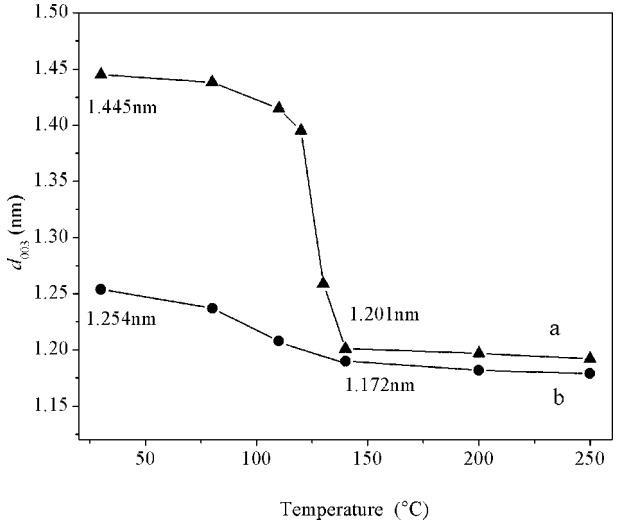

Figure 7. Relationship between *d*(003) basal spacing and temperature for (a) LDH-2.0-[ZnY] and (b) LDH-3.0-[ZnY].

cause the bilayer $[ZnY]^{2-}$ to adopt a thermodynamically more stable monolayer orientation. Pillar reorientation at 140 °C, therefore, appears to be responsible for the observed gallery contraction of 0.244 nm for the LDH-2.0-[ZnY]. In the case of LDH-3.0-[ZnY], the relative intensities of the (00*l*) reflections are almost unchanged with increasing temperature, confirming that the orientation of $[ZnY]^{2-}$ in the interlayer galleries of LDH-3.0-[ZnY] does not vary with temperature. In addition, a weak shoulder on the (006) reflection peak centered at $2\theta \approx 12°$ in the pattern for LDH-3.0-[ZnY] gradually disappears with increasing temperature, indicating that the small amount of bilayer phase initially present is completely converted into the monolayer form.

The monolayer structure in LDH–[ZnY] is retained on heating up to 300 °C. On further heating above 300 °C, however, the absence of (00*l*) diffraction peaks corresponding to an LDH phase indicates that the layer structure is completely destroyed. This is consistent with TGA-MS data (see below), which suggest that dehydroxylation of the brucite-like layers along with anion decomposition occurs above 300 °C. At 400 °C, reflections characteristic of a cubic MgO-like phase begin to appear and at 900 °C reflections from an $MgAl_2O_4$ spinel phase and MgO are present, as is generally observed for calcined MgAl LDHs.[48] In addition, peaks that can be assigned to ZnO (JCPDS Card 01-1136), resulting from the decomposition of $[ZnY]^{2-}$, can be observed.

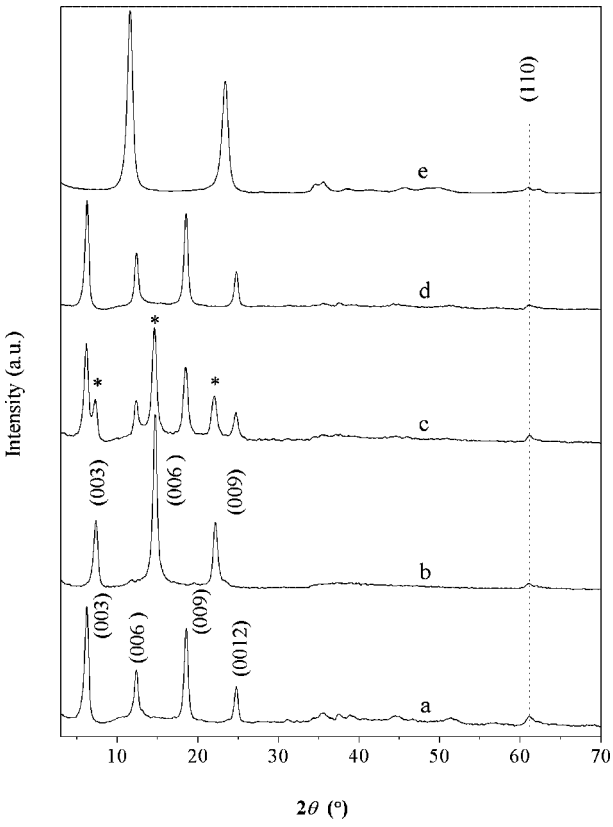

Figure 8. Powder XRD patterns of LDH-2.0-[ZnY] at (a) room temperature, (b) 140 °C, (c) room temperature (after cooling the sample from 140 °C in moist air for 20 min), (d) room temperature (after cooling the sample from 140 °C in moist air for 1 h), and (e) LDH–CO_3–[ZnY].

A Reversible Structural Transformation

Although we have suggested above that the origin of the observed metastable phase is a reorientation of the $[MY]^{2-}$ anion in the interlayers, the possibility remains that it could be because of grafting of the anion to the hydroxyl layers as has been claimed by some authors for other anions in describing the formation of similar metastable phases associated with a significant interlayer contraction.[19–24] In order to provide further insight into the origin of the metastable phase, a sample of LDH-2.0-[ZnY] was heated to 140 °C and, after recording the powder XRD pattern at this temperature, subsequently cooled to room temperature over either 20 min or 1 h (in moist air), and the powder XRD patterns measured again (see Figure 8). The results show that the original phase and the metastable phase coexist when the sample is cooled in moist air for 20 min (Figure 8c), indicating that the structural transformation is reversible upon hydration. When the hydration reaction time is extended to 1 h the structural transformation is completely reversed as shown by the disappearance of peaks associated with the metastable phase (Figure 8d).

The recovery of the original phase on cooling demonstrates that heat treatment (up to 140 °C) does not result in covalent grafting of the anions to the hydroxyl layers. The absence of grafting is further confirmed by the observation that the $[MY]^{2-}$ anions in the metastable phase are readily exchanged with carbonate anions (Figure 8e). This would not be expected to be the case if the ions were actually grafted to the layers. The reversible structural transformation observed on heating and cooling is shown schematically in Figure 9.

To further study the evolution of the interlayer arrangement in this reversible transition the thermal behavior of LDH-2.0-[ZnY] was investigated by TGA, coupled with mass spectrometry. The TGA curves, as well as the analysis of the evolved decomposition products by mass spectrometry, are presented in Figure 10. Generally, four steps are observed in the thermal evolution of LDHs: desorption of physically adsorbed water, removal of the interlayer structural water, dehydroxylation of the brucite-like sheets, and the decomposition of the interlayer anions, although the first two steps may overlap in the low-temperature range. The thermal decomposition of LDH-2.0-[ZnY] is indeed characterized by three mass-loss steps. The first one from room temperature to 300 °C corresponds to the removal of surface adsorbed water and interlayer water molecules with their respective DTG peaks centered at 88 and 134 °C. The coupled mass spectrometry confirms this result since the ion current peak (m/z = 18 $[H_2O^+]$) is assigned to the evolution of water. The temperature range of the loss of interlayer water is similar to that associated with the large contraction associated with guest reorientation (see Figure 5). This suggests that loss of water molecules may play an im-

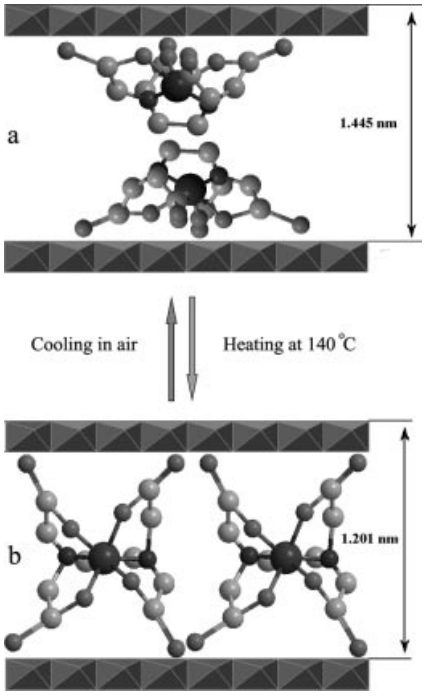

Figure 9. Schematic illustration of the reversible structural transformation of LDH-2.0-[ZnY] at (a) room temperature and (b) 140 °C.

portant role in initiating the reorientation. The sharp mass loss observed in the range 300–600 °C is due to the dehydroxylation of the brucite-like layers as well as combustion of the organic materials, with a corresponding sharp peak centered at 396 °C in the DTG curve (Figure 10a). This is confirmed by the mass spectrometry results (Figure 10b), which show strong CO_2^+, NO^+, and H_2O^+ ion currents over the entire decomposition range. The final gradual mass loss in the range 600–950 °C is a result of the oxidation of residual organic material as shown by the evolution of CO_2 alone in the MS trace. The thermal decomposition data is in good agreement with the in-situ HT-XRD data discussed above.

The in-situ FT-IR spectra of LDH-2.0-[ZnY] heated in the temperature range 30–550 °C are shown in Figure 11, and are also indicative of a reorientation taking place upon heating rather than a grafting process. On heating, the first change in the FT-IR spectra occurs between 30 and 150 °C. The band at 3444 cm^{-1} moves to a higher frequency (3506 cm^{-1}) and its intensity decreases. This may be attributed to an increase in the force constant of the OH bond as a result of the loss of hydrogen bonding with interlayer

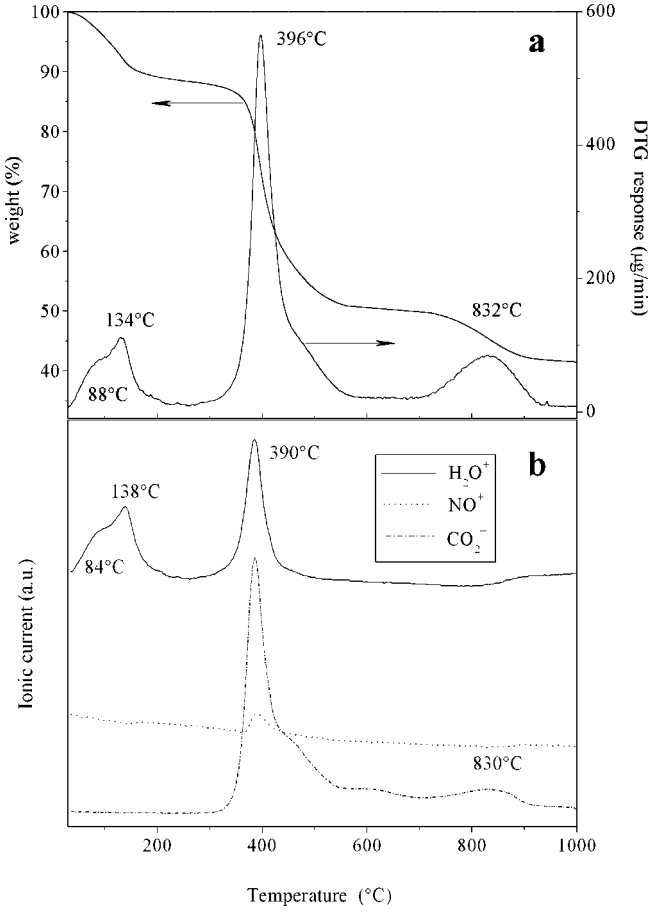

Figure 10. TGA curve (a) and coupled mass spectrometry trace (b) for LDH-2.0-[ZnY].

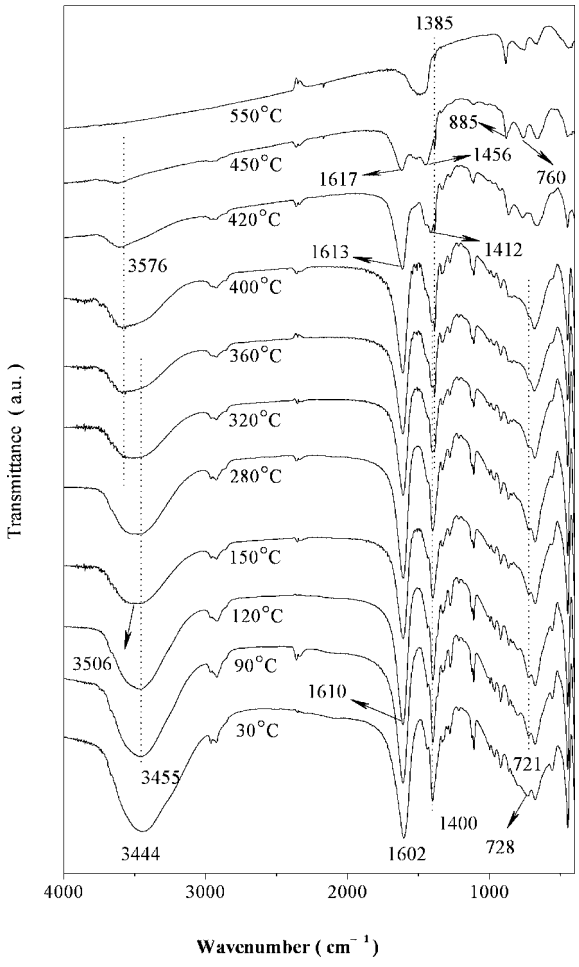

Figure 11. In-situ variable-temperature FT-IR spectra of LDH-2.0-[ZnY].

water. The asymmetric and symmetric stretching vibrations of the carboxylate group show slight shifts to higher frequency and lower frequency, respectively. As discussed above, the wavenumber difference $\Delta\nu = \nu_{as} - \nu_s$ gives information about the coordination environment of the carboxylate group. The value of $\Delta\nu$ shows only a marginal increase, from 202 cm^{-1} at 30 °C to 210 cm^{-1} at 150 °C, which suggests that the coordination environment of the carboxylate group remains nearly unaffected; this is consistent with the proposed reorientation of the $[ZnY]^{2-}$ anions on heating. If the carboxylate groups actually became covalently grafted to the hydroxyl layers a much more dramatic change in the value of $\Delta\nu$ would be expected.[23]

On heating from 320 to 550 °C there is a gradual decrease in the intensity of hydroxyl and carboxylate vibration bands, consistent with the dehydroxylation and decomposition processes observed by TGA-MS in this temperature range. The emergence of bands at 885 and 760 cm^{-1} above 450 °C can be assigned to M–O vibrations in mixed oxide phases.

Conclusions

Highly ordered MgAl LDHs intercalated by $[MY]^{2-}$ guest anions have successfully been prepared by a hydrothermal synthesis method. Charge matching between the $[MY]^{2-}$ anions and the LDH layers controls the gallery orientation of the $[MY]^{2-}$ anions. In the case of LDH-2.0-[MY], the interlayer separation for the fully hydrated material indicates that the guest species are arranged in a bilayer with the minimal dimension perpendicular to the host layers. In contrast, in LDH-3.0-[MY] the guest species are arranged in a monolayer with the maximal dimension tilted with respect to the host layers. Heating LDH-2.0-[MY] at 140 °C results in a reorientation of the $[MY]^{2-}$ complex in the interlayer giving a similar monolayer structure to that found in LDH-3.0-[MY]. The metastable monolayer phase is quite stable and the layered structure can still be identified by powder XRD after heat treatment at 300 °C. Rehydration of the calcined solids upon cooling to room temperature in air leads to the recovery of materials with the original values of the gallery heights. The reversible nature of the transformation is inconsistent with a grafting process and strongly supports a mechanism involving reorientation of the anion in the interlayer galleries. Calcination at 400 °C gives rise to a collapse of the layered structure and amorphous phases are formed. Further heat treatment of LDH-2.0-MY leads to a mixture of MgO, MO, and $MgAl_2O_4$ spinel phases above 750 °C.

Experimental Section

Synthesis

Preparation of $Na_2[MY]\cdot xH_2O$: The $Na_2[MY]\cdot xH_2O$ (M = Zn, Ni, Co, Cu; Y = $edta^{4-}$) complexes were prepared by mixing the appropriate molar equivalents of aqueous solutions of the corresponding metal nitrate, $Na_2C_{10}H_{14}N_2O_8\cdot 2H_2O$ (Na_2H_2Y), and Na_2CO_3, which is similar to the method described by Sawyer and Paulsen.[49] The resulting solution was adjusted to pH = 7.0 with dilute HNO_3 solution and warmed to boiling point. After concentration of the solution to one-third of the initial volume, absolute ethanol was added until a slight turbidity appeared. Finally, the solution was cooled in a refrigerator. The resulting crystalline material was filtered and recrystallized from a water/ethanol mixture. The recrystallized complexes were isolated by filtration and dried under air.

Preparation of LDH–Nitrate Precursor: MgAl–NO_3 LDH with different Mg/Al molar ratios (designated LDH-*X*-NO_3, where *X* = value of Mg/Al molar ratios in the mixed solution) were prepared by a coprecipitation method at controlled pH as described in the literature.[50] These preparations were carried out under constant nitrogen flow using freshly decarbonated, deionized water. Mixed solutions of $Mg(NO_3)_2$ and $Al(NO_3)_3$ with the required Mg/Al molar ratio, having total cation concentrations equal to 1 M, have been used at constant pH = 9.5. After precipitation, the suspension was aged at 100 °C for 8 h while stirring. The resulting white precipitate was collected by centrifugation, washed several times with carbonate-free deionized water, and dried in air at 50 °C for 24 h.

Preparation of $[MY]^{2-}$-Intercalated MgAl LDH: LDH-2.0-[MY] was obtained by anion exchange of the LDH-2.0-NO_3 precursors under hydrothermal conditions. As an example, the intercalation of the $[NiY]^{2-}$ anion into the LDH-2.0-NO_3 precursor is described. In the first step, a mixture of the LDH precursor (0.550 g, 0.002 mol) and $Na_2[NiY]\cdot 3H_2O$ (1.788 g, 0.004 mol) in a twofold molar excess over the anion exchange capacity was crushed in an agate mortar for 5 min and placed in an autoclave (22 cm^3) with distilled and decarbonated water (20 cm^3). The autoclave was then heated at 120 °C for 24 h developing an autogenous pressure. The powdered products were collected by centrifugation, washed three times with carbonate-free deionized water, and finally dried in air at 50 °C for 24 h. Other LDH-*X*-[ZnY] materials were obtained by the same procedure using the corresponding LDH-*X*-NO_3 precursors and $Na_2[ZnY]\cdot xH_2O$.

Characterization

Elemental analyses for metals were performed by inductively coupled plasma (ICP) emission spectroscopy with a Shimadzu ICPS-7500 instrument using solutions prepared by dissolving the samples in dilute HNO_3. C, H, and N analyses were carried out using an Elementarvario elemental analysis instrument. The in-situ powder X-ray diffraction (in-situ XRD) data were recorded with a Shimadzu XRD-6000 powder diffractometer over the temperature range 30–900 °C in air, using Cu-K_α radiation (λ = 0.154 nm) at 40 kV and 30 mA. The samples, as unoriented powders, were step-scanned in steps of 5°/min in the 2θ range from 3 to 70° using a count time of 4 s per step. The rate of temperature increase was 10 °C/min with a holding time of 5 min before each measurement. The in situ Fourier transform infrared (in-situ FT-IR) spectra were recorded with a Nicolet 605XB FT-IR spectrometer in the range 4000–400 cm^{-1} with 4 cm^{-1} resolution under flowing N_2 (65 cm^3/min) with a heating rate of 5 °C/min in the range 25–450 °C. The KBr pellet technique, with a typical pellet containing ca. 1 wt% sample in KBr, was employed. Thermogravimetric analysis coupled to mass spectrometry was performed using a Perkin–Elmer Diamond TG apparatus linked to a ThermoStar mass spectrometer by a quartz capillary transfer line heated at 190 °C. The heating rate was 10 °C/min with an N_2 flow rate of 200 cm^3/min. The TG apparatus was at atmospheric pressure, and the mass spectrometer at a working pressure of 6×10^{-6} Torr. The mass of sample used was 10 mg in each case.

Acknowledgments

We are grateful to the National Natural Science Foundation of China (Grant No. 20401002) and to the National Natural Science Foundation Major International Joint Research Program (Project No. 20620130108).

[1] *Layered Double Hydroxides: Present and Future* (Ed.: V. Rives), Nova Science Publishers Inc., New York, **2001**. pp. 251–431.
[2] P. Beaudot, M. E. De Roy, J. P. Besse, *Chem. Mater.* **2004**, *16*, 935–945.
[3] A. V. Lukashin, A. A. Vertegel, A. A. Eliseev, M. P. Nikiforov, P. Gornert, Y. D. Tretyakov, *J. Nanopart. Res.* **2003**, *5*, 455–464.
[4] S. Gago, M. Pillinger, R. A. Sá Ferreira, L. D. Carlos, T. M. Santos, I. S. Gonçalves, *Chem. Mater.* **2005**, *17*, 5803–5809.
[5] V. Rives, M. A. Ulibarri, *Coord. Chem. Rev.* **1999**, *181*, 61–115.
[6] K. A. Tarasov, D. O'Hare, V. P. Isupov, *Inorg. Chem.* **2003**, *42*, 1919–1927.
[7] A. I. Tsyganok, T. Tsunoda, S. Hamakawa, K. Suzuki, K. Takehira, T. Hayakawa, *J. Catal.* **2003**, *213*, 191–203.
[8] C. Li, G. Wang, D. G. Evans, X. Duan, *J. Solid State Chem.* **2004**, *177*, 4569–4575.
[9] A. I. Tsyganok, M. Inaba, T. Tsunoda, S. Hamakawa, K. Suzuki, T. Hayakawa, *Catal. Commun.* **2003**, *4*, 493–498.
[10] A. I. Tsyganok, K. Suzuki, S. Hamakawa, K. Takehira, T. Hayakawa, *Catal. Lett.* **2001**, *77*, 75–86.
[11] K. A. Tarasov, V. P. Isupov, B. B. Bokhonov, Y. A. Gaponov, B. P. Tolochko, M. R. Sharafutdinov, S. S. Shatskaya, *J. Mater. Synth. Process.* **2000**, *8*, 21–27.
[12] V. P. Isupov, R. P. Mitrofanova, L. E. Chupakhina, E. V. Starikova, K. A. Tarasov, M. M. Yulikov, *J. Struct. Chem.* **2005**, *46* (suppl.), S165–S170.
[13] E. V. Starikova, V. P. Isupov, K. A. Tarasov, L. E. Chupakhina, M. M. Yulikov, *J. Struct. Chem.* **2004**, *45* (suppl.), S115–S120.
[14] M. R. Perez, I. Pavlovic, C. Barriga, J. Cornejo, M. C. Hermosin, M. A. Ulibari, *Appl. Clay Sci.* **2006**, *32*, 245–251.
[15] L. Ukrainczyk, M. Chibwe, T. J. Pinnavaia, S. A. Boyd, *J. Phys. Chem.* **1994**, *98*, 2668–2676.
[16] N. Iyi, K. Kurashima, T. Fujita, *Chem. Mater.* **2002**, *14*, 583–589.
[17] U. Costantino, N. Coletti, M. Nocchetti, G. G. Aloisi, F. Elisei, *Langmuir* **1999**, *15*, 4454–4460.
[18] T. Itoh, T. Shichi, T. Yui, H. Takahashi, Y. Inui, K. Takagi, *J. Phys. Chem. B* **2005**, *109*, 3199–3206.
[19] C. Vaysse, L. Guerlou-Demourgues, C. Delmas, *Inorg. Chem.* **2002**, *41*, 6905–6913.
[20] F. Malherbe, J. P. Besse, *J. Solid State Chem.* **2000**, *155*, 332–341.
[21] M. Del Arco, D. Carriazo, S. Gutiérrez, C. Martín, V. Rives, *Inorg. Chem.* **2004**, *43*, 375–384.
[22] C. Vaysse, L. Guerlou-Demourgues, A. Demourgues, C. Delmas, *J. Solid State Chem.* **2002**, *167*, 59–72.
[23] V. Prévot, C. Forano, J. P. Besse, *Appl. Clay Sci.* **2001**, *18*, 3–15.
[24] L. Vieille, I. Rousselot, F. Leroux, J. P. Besse, C. Taviot-Guého, *Chem. Mater.* **2003**, *15*, 4361–4368.
[25] T. Hibino, A. Tsunashima, *Chem. Mater.* **1997**, *9*, 2082–2089.
[26] D. Carriazo, C. Domingo, C. Martín, V. Rives, *Inorg. Chem.* **2006**, *45*, 1243–1251.
[27] S. Gago, M. Pillinger, T. M. Santos, J. Rocha, I. S. Gonçalves, *Eur. J. Inorg. Chem.* **2004**, 1389–1395.
[28] J. J. Bravo-Suárez, E. A. Páez-Mozo, S. T. Oyama, *Chem. Mater.* **2004**, *16*, 1214–1225.
[29] S. K. Yun, T. J. Pinnavaia, *Inorg. Chem.* **1996**, *35*, 6853–6860.
[30] V. Prévot, C. Forano, J. P. Besse, *Inorg. Chem.* **1998**, *37*, 4293–4301.
[31] A. Tsyganok, A. Sayari, *J. Solid State Chem.* **2006**, *179*, 1830–1841.
[32] M. A. Porai-Koshits, T. N. Polynova, *Koord. Khim.* **1984**, *10*, 725–772.
[33] H. A. Weakliem, J. L. Hoard, *J. Am. Chem. Soc.* **1959**, *81*, 549–555.
[34] F. M. Labajos, V. Rives, M. A. Ulibarri, *J. Mater. Sci.* **1992**, *27*, 1546–1552.
[35] Z. P. Xu, H. C. Zeng, *J. Phys. Chem. B* **2001**, *105*, 1743–1749.
[36] V. Rives, in: *Layered Double Hydroxides: Present and Future* (Ed.: V. Rives), Nova Science Publishers Inc., New York, **2001**, pp. 139–192.
[37] K. Nakamoto, *Infrared and Raman Spectra of Inorganic and Coordination Compounds*, 4th ed., Wiley, New York, **1986**, pp. 231–248.
[38] G. B. Deacon, R. J. Phillips, *Coord. Chem. Rev.* **1980**, *33*, 227–250.
[39] N. Gutmann, B. Müller, H. J. Tiller, *J. Solid State Chem.* **1995**, *119*, 331–338.
[40] Y. Tomita, K. Ueno, *Bull. Chem. Soc. Jpn.* **1963**, *36*, 1069–1073.
[41] F. Kooli, I. C. Chisem, M. Vucelic, W. Jones, *Chem. Mater.* **1996**, *8*, 1969–1977.
[42] M. Kaneyoshi, W. Jones, *J. Mater. Chem.* **1999**, *9*, 805–811.
[43] S. Bonnet, C. Forano, A. De Roy, J. P. Besse, *Chem. Mater.* **1996**, *8*, 1962–1968.
[44] M. Del Arco, S. Gutiérrez, C. Martín, V. Rives, *Inorg. Chem.* **2003**, *42*, 4232–4240.
[45] G. Q. Wu, L. Y. Wang, D. G. Evans, X. Duan, *Eur. J. Inorg. Chem.* **2006**, 3185–3196.
[46] Q. Yuan, M. Wei, D. G. Evans, X. Duan, *J. Phys. Chem. B* **2004**, *108*, 12381–12387.
[47] R. Allmann, *Acta Crystallogr., Sect. B* **1968**, *24*, 972–977.
[48] B. Rebours, J. B. d'Espinose de la Caillerie, O. Clause, *J. Am. Chem. Soc.* **1994**, *116*, 1707–1717.
[49] D. T. Sawyer, P. J. Paulsen, *J. Am. Chem. Soc.* **1959**, *81*, 816–820.
[50] S. Miyata, *Clays Clay Miner.* **1975**, *23*, 369–375.

Received: October 6, 2006
Published Online: January 4, 2007

